UWB/IMU Fusion Localization Strategy Based on Continuity of Movement

Li Zhang[1(✉)], Jinhui Bao[1], Jingao Xu[2], and Danyang Li[2]

[1] HeFei University of Technology, Hefei 230000, China
lizhang@hfut.edu.cn
[2] Tsinghua University, Beijing 100000, China

Abstract. Commercial and industrial sectors are increasingly deploying inertial measurement unit (IMU) and ultrawideband (UWB) for motion control, automation, and positioning applications, such as intelligent manufacturing, smart homes and smartphones. However, it does not perform well in a multi-obstacle environment, such as the problem of locating workers in a multi-worker environment and finding cars in a large parking lot. This is because IMU can provide a low-cost and accurate inertial navigation solution in a short time, but its positioning error increases rapidly over time as a result of accumulated accelerometer measurement errors. On the other hand, even under line-of-sight (LOS) settings, UWB positioning and navigation accuracy is impacted by the real environment, resulting in unreliable leaps. Therefore, it is difficult to achieve high accuracy positioning using single positioning and navigation system in indoor environments. In this paper, a robust UWB and IMU fusion indoor localization system based on adaptive dynamic Kalman Filter (ADKF) algorithm has been proposed which relies on motion continuity and can be applied to indoor complex multipath environment. Specifically, in order to mitigate non-line-of-sight (NLOS) errors, one novel range-constrained weighted least square (RWLS) algorithm is presented. The experimental results show that both algorithms can mitigate NLOS errors effectively and reach a particular degree of robustness and ongoing tracking capability in integrated indoor positioning system (IPS).

Keywords: Kalman Filter (KF) · inertial measurement unit (IMU) · ultrawideband (UWB) · indoor positioning system (IPS)

1 Introduction

The accuracy of current navigation systems, such as the Global Positioning System (GPS) and the Global Navigation Satellite System (GLONASS), is high

Supported by the National Key Research and Development Program (2018YFB2100301); National Natural Science Foundation of China (61972131).

S. Longfei and P. Bodhi (Eds.): MobiQuitous 2022, LNICST 492, pp. 65–78, 2023.
https://doi.org/10.1007/978-3-031-34776-4_4

when used outdoors but very low when used indoors [1]. As a result, precise indoor localization and tracking have gained popularity and given rise to a number of applications, including augmented reality, intelligent advertising, and customer navigation. Recent publications of a wealth of research [2–10] demonstrate the growing interest in indoor location and tracking systems, which employ wireless signals, cameras, inertial measurement units (IMU), ultrawideband (UWB), etc.

IMU is the core of the inertial navigation system (INS) including a three-axis accelerometer and gyroscope [11]. The attitude information and motion characteristics of the object, such as acceleration, angular velocity and angle can be acquired by IMU [12]. The position of the carrier can be directly determined by mathematically integrating the acceleration without the use of a reference base station. Due to its low cost, minimal influence on the environment, and high accuracy in a short time, INS is frequently employed in moving target placement and navigation scenarios for aircraft, automobiles, pedestrians, and other moving targets; nevertheless, the error grows quickly with time [13]. Additionally, many indoor positioning systems use ultra-wideband (UWB) technology [14], constructing several non-visual distance processing techniques, such as the channel model [15], multipath component estimate [16], and theoretical lower band of positioning errors [17].

Utilizing nanosecond non-sinusoidal narrow pulse transmissions, UWB is a successful communication technology for position-sensing sensor networks [18]. Achieving centimeter-level range precision, UWB benefits from short pulse intervals, high time resolution, and robustness to the multipath effect [19,20]. Due to its high-frequency spectrum, UWB is only appropriate for a line-of-sight situation. When object occlusion occurs, the range accuracy of UWB is significantly decreased. As can be observed, employing simply IMU or UWB to obtain high accuracy in complicated indoor conditions is challenging.

To achieve high robustness and accuracy of the indoor localization system, this article focuses on the integration of IMU and UWB based on Kalman Filter technique. We propose a RWLS algorithm based on the distance constraint for UWB positioning and then an ADKF algorithm combining IMU and UWB based on motion continuity. Extensive experiments show that both algorithms can mitigate NLOS errors effectively and reach a particular degree of robustness and ongoing tracking capability in indoor complex and dynamic environments.

The main contributions are summarized as follows:

- We propose a RWLS algorithm based on the distance constraint, which can mitigate NLOS errors.
- A loosely coupled ADKF tracking algorithm is proposed to combine IMU and UWB, which can effectively reduce uncertain jumping caused by complex indoor environment.
- Extensive real-world experiments are performed to validate our algorithms. The experimental results show that our algorithms perform better in dynamic and complex indoor environments.

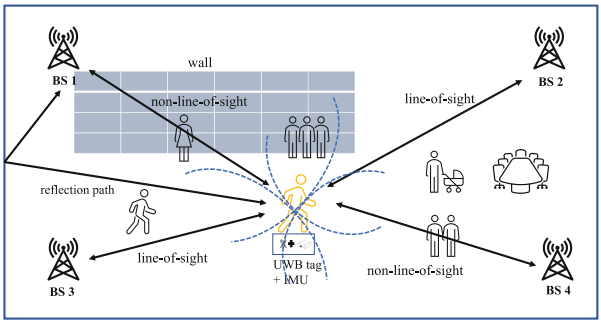

Fig. 1. Positioning in a complex indoor multipath environment.

2 Related Work

Complementary characteristics of IMU and UWB are considered to improve positioning accuracy. An improved PDR/UWB integrated system is proposed based on the variable noise variance (VNV) Kalman Filter algorithm to dynamically adjust the noise distribution through a non-line-of-sight evaluation function [21]. An integrated indoor positioning system (IPS) combining IMU and UWB is proposed through the extended Kalman Filter (EKF) and unscented Kalman Filter (UKF) to improve the robustness and accuracy [22]. The federated derivative cubature Kalman Filter (FDCKF) method is proposed by combining the traditional Kalman Filter and the cubature Kalman Filter then the observations of the UWB and the IMU can be effectively fused [23].

The algorithms proposed by predecessors can be applied to industrial robots, power plant positioning technology, judicial prisons, industrial warehouses and other relatively simple environments. However, in complex environments such as large parking lots and factories with a large number of workers, multi-path effect and non-line-of-sight effect will lead to poor location results.

3 Single Sensor Positioning Algorithm

In this section, we first introduce the IMU-based and UWB-based positioning algorithms, and propose a range-constrained weighted least square (RWLS) into UWB localization algorithm. The IMU sensor consists of a three-axis accelerometer and gyroscope. The UWB sensors consist of four base stations (BSs) with known positions and an unknown position tag.

3.1 Inertial Sensor Positioning Algorithm

The updating of the attitude matrix calculation in the strap-down INS (SINS) and the transformations of various coordinate systems have both received a lot of attention [24].

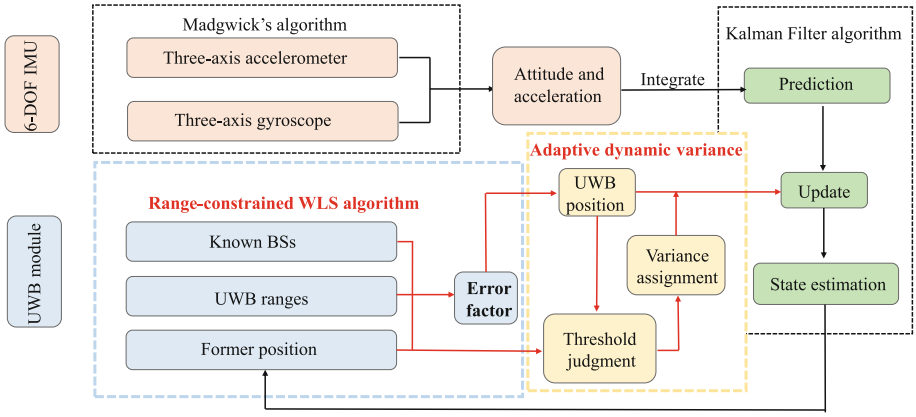

Fig. 2. System Overview.

It is crucial to use the suitable coordinate system in order to accurately characterize the tag's space motion state. Assume that the world coordinate system is $Ox_wy_wz_w$ and that $Ox_by_bz_b$ represents the body coordinate system, respectively. The attitude matrix of the carrier is the coordinate transformation matrix between the world coordinate system and the body coordinate system. The coordinates of the accelerometer and gyroscope in the system belong to the body coordinate system. While the world coordinate system is where the final results of acceleration, velocity, and position belong. Madgwick's algorithm [25] is considered to solve this problem of its low computational cost. Then the rotation matrix R can be obtained from the three-axis acceleration and gyroscope data. The acceleration in the body coordinate system, $\boldsymbol{a^b}$ is expressed in Eq. (1).

$$\boldsymbol{a^b} = \begin{bmatrix} a_x^b & a_y^b & a_z^b \end{bmatrix}^T \tag{1}$$

Thus, the acceleration in the world coordinate system, $\boldsymbol{a^{w1}}$, can be obtained by the coordinate transformation:

$$\boldsymbol{a^{w1}} = \begin{bmatrix} a_x^{w1} & a_y^{w1} & a_z^{w1} \end{bmatrix}^T = R\boldsymbol{a^b}. \tag{2}$$

After subtracting the gravitational acceleration, the acceleration is $\boldsymbol{a^w}$:

$$\boldsymbol{a^w} = \begin{bmatrix} a_x^w \\ a_y^w \\ a_z^w \end{bmatrix} = \begin{bmatrix} a_x^{w1} \\ a_y^{w1} \\ a_z^{w1} \end{bmatrix} - \begin{bmatrix} 0 \\ 0 \\ g \end{bmatrix}. \tag{3}$$

Let $\boldsymbol{v^w\ (t_j)}$ represents the velocity in the world coordinate system at the time t_j. Then, the velocity in the world coordinate system at the time t_{j+1}, $\boldsymbol{v^w\ (t_{j+1})}$, can be acquired by using the acceleration integral as shown below.:

$$\begin{bmatrix} v_x^w\ (t_{j+1}) \\ v_y^w\ (t_{j+1}) \\ v_z^w\ (t_{j+1}) \end{bmatrix} = \begin{bmatrix} v_x^w\ (t_j) \\ v_y^w\ (t_j) \\ v_z^w\ (t_j) \end{bmatrix} + \begin{bmatrix} a_x^w \\ a_y^w \\ a_z^w \end{bmatrix} \Delta t \tag{4}$$

Let $\boldsymbol{P^w\ (t_j)}$ represents the position in the world coordinate system at the time t_j, and then the position in the world coordinate system at the time t_{j+1}, $\boldsymbol{P^w\ (t_{j+1})}$, can be calculated as follows:

$$\begin{bmatrix} P_x^w\ (t_{j+1}) \\ P_y^w\ (t_{j+1}) \\ P_z^w\ (t_{j+1}) \end{bmatrix} = \begin{bmatrix} P_x^w\ (t_j) \\ P_y^w\ (t_j) \\ P_z^w\ (t_j) \end{bmatrix} + \begin{bmatrix} v_x^w \\ v_y^w \\ v_z^w \end{bmatrix} \Delta t + \frac{1}{2} \begin{bmatrix} a_x^w \\ a_y^w \\ a_z^w \end{bmatrix} \Delta t^2. \tag{5}$$

3.2 Ultra-wideband Positioning Algorithm

The ranging-based technique is typically used in the two-step UWB positioning approach. Measuring the distances between the unknown node and anchor nodes is the first step. The position of the unknown node is determined in the second phase by using distance information.

In our approach to range measuring, we employ the SDS-TWR optimization algorithm [26]. We use multilateration to establish the tag's position depending on the distance once the range measurements are finished. In particular, Fig. 1 illustrates a multilateration case in which the separations between the tag and four BSs are assessed. The tag should ideally be situated near the intersection of four circles centered on four BSs in the 2-D plane. Due to range error, particularly in the non-line-of-sight range, the intersection is typically not singular.

Suppose that the coordinates of unknown tag and the ith BS are (x, y) and (x_i, y_i), respectively. Then, the real distance between the unknown tag and the ith BS, d_i can be written as $\sqrt{(x_i - x)^2 + (y_i - y)^2}$. The distance between the mobile tag and the ith BS is d_i'. Therefore, the difference between the actual distance and measured distance is calculated by $\rho_i = d_i - d_i'$. We use the traditional LS approach to minimize the value of $\sum_{i=1}^{n} \rho_i^2$ to cope with the range noise. For each distance, the following equations are used to calculate the position of an unknown tag:

$$\begin{cases} d_1^2 = (x_1 - x)^2 + (y_1 - y)^2 \\ d_2^2 = (x_2 - x)^2 + (y_2 - y)^2 \\ \quad\quad \vdots \\ d_n^2 = (x_n - x)^2 + (y_n - y)^2 \end{cases}. \tag{6}$$

Let's remove the first equation from all the others to get

$$AX = b, \tag{7}$$

where

$$A = \begin{bmatrix} x_2 - x_1 & y_2 - y_1 \\ x_3 - x_1 & y_3 - y_1 \\ \vdots & \vdots \\ x_n - x_1 & y_n - y_1 \end{bmatrix}, X = \begin{bmatrix} x \\ y \end{bmatrix}$$
$$b = \frac{1}{2} \begin{bmatrix} x_2^2 + y_2^2 - d_2^2 - \left(x_1^2 + y_1^2 - d_1^2\right) \\ x_3^2 + y_3^2 - d_3^2 - \left(x_1^2 + y_1^2 - d_1^2\right) \\ \vdots \\ x_n^2 + y_n^2 - d_n^2 - \left(x_1^2 + y_1^2 - d_1^2\right) \end{bmatrix}. \tag{8}$$

Every range value in the LS approach has the same weight. The fact that the range error varies on each side makes it obvious that it is not very appropriate. The weighted least square (WLS) [22] approach was suggested by Daquan Feng et al. to address the issue. When the tag is nearer the BS during the ranging process, it is believed that the ranging error is lower. As a result, adopting a heavier weight for the smaller range value further reduces positioning error. The reciprocal of the ranging value d yields the weighting coefficient η as follows:

$$\eta = \begin{bmatrix} \frac{1}{d_2} & 0 & 0 & 0 \\ 0 & \frac{1}{d_3} & 0 & 0 \\ 0 & 0 & \ddots & 0 \\ 0 & 0 & 0 & \frac{1}{d_n} \end{bmatrix}. \tag{9}$$

Then, the WLS solution of X is calculated as follows:

$$X = \left(A^T \eta A\right)^{-1} A^T \eta b. \tag{10}$$

In actual environments, due to the complexity of space and the movement of pedestrians, the view that the closer the tag is to the BS, the smaller the ranging error may be untrue. Thus, we propose the range-constrained weighted least square (RWLS) algorithm based on the former position constraint to solve this problem. Due to the short sampling time of UWB, there is no obvious position change between two adjacent sampling points, which means continuity of movement. Assuming that $X_{t_{j-1}}$ is the former position, we introduce the ranging error factor $\Delta m_{i,j}$, which is the ranging error of the ith base station at the time t_j.

$$\Delta m_{i,j} = \left|\mathrm{dis}\left(X_{t_{j-1}}, (x_i, y_i)\right) - d_{i,j}\right|, \tag{11}$$

where dis() represents the distance between two points and $d_{i,j}$ mean the measured distance from the tag to the ith BS at the time t_j. The error factor and $d_{i,j}$ is normalized as follows:

$$\begin{aligned} \Delta m_{i,j} &= \frac{\Delta m_{i,j}}{\sum_{i=1}^{n} \Delta m_{i,j}} \\ d_{i,j} &= \frac{d_{i,j}}{\sum_{i=1}^{n} d_{i,j}}. \end{aligned} \tag{12}$$

We assign a higher weight for the smaller ranging error factor and smaller range d, the positioning accuracy will be further improved. Then we can get a new matrix of coefficients η_{new} as follows:

$$\eta_{\text{new}} = \begin{bmatrix} \frac{1}{\Delta m_{2,j} d_{2,j}} & 0 & 0 & 0 \\ 0 & \frac{1}{\Delta m_{3,j} d_{3,j}} & 0 & 0 \\ & & \ddots & \\ 0 & 0 & & 0 \\ 0 & 0 & 0 & \frac{1}{\Delta m_{n,j} d_{n,j}} \end{bmatrix}. \tag{13}$$

Finally, the positioning result at the time t_j is obtained:

$$X_{t_j} = \left(A^T \eta_{\text{new}}\, A\right)^{-1} A^T \eta_{\text{new}}\, b. \tag{14}$$

The complete RWLS algorithm is shown in **RWLS algorithm**.

RWLS algorithm

Input: $n, m, (x_i, y_i), X_{t_{j-1}}, d_{i,j}$

1: n = numbers of BSs
m = numbers of UWB samples

2 : for j from 1 to m

3: **Initialization**

if $j = 1$:

$$\eta = \begin{bmatrix} \frac{1}{d_{2,1}} & 0 & 0 & 0 \\ 0 & \frac{1}{d_{3,1}} & 0 & 0 \\ & & \ddots & \\ 0 & 0 & & 0 \\ 0 & 0 & 0 & \frac{1}{d_{n,1}} \end{bmatrix}$$

else:

4: **Calculate error factor**

for i from 1 to n :

$$\Delta m_{i,j} = \left|\text{dis}\left(X_{t_{j-1}}, (x_i, y_i)\right) - d_{i,j}\right|$$

5: **Normalized**

$$\Delta m_{i,j} = \frac{\Delta m_{i,j}}{\sum_{i=1}^{n} m_{i,j}} \quad d_{i,j} = \frac{d_{i,j}}{\sum_{i=1}^{n} d_{i,j}}$$

6: **New coefficient matrix**

$$\eta = \begin{bmatrix} \frac{1}{\Delta m_{2,j} d_{2,j}} & 0 & 0 & 0 \\ 0 & \frac{1}{\Delta m_{3,j} d_{3,j}} & 0 & 0 \\ & & \ddots & \\ 0 & 0 & & 0 \\ 0 & 0 & 0 & \frac{1}{\Delta m_{n,j} d_{n,j}} \end{bmatrix}$$

end

7: **Position**

$$X_{t_j} = \left(A^T \eta A\right)^{-1} A^T \eta b$$

end

Output: P_{t_j}

4 Fusion Algorithm Based on UWB and IMU

It is known that the linear Kalman Filter can calculate the ideal carrier state in the linear Gaussian model, provided that the noise from the IMU and UWB sensors is independent of one another and that both abide by the Gaussian distribution with zero mean and variance σ^2. In this section, we propose an adaptive dynamic Kalman Filter (ADKF) algorithm based on the distance constraint. The design of an indoor positioning system based on the combination of IMU and UWB is shown in Fig. 2.

We first use UWB to provide the initial position X_0 by RWLS algorithm and initial velocity, $V_x = V_y = 0$. The state vector of the tag is $\hat{X}_{k-1}$ as follows:

$$\hat{X}_{k-1} = \begin{bmatrix} P_x \\ P_y \\ V_x \\ V_y \end{bmatrix}. \tag{15}$$

Assuming that the tag motion satisfies the uniformly accelerated motion model in a short time, we predict the state $\hat{X}_{k|k-1}$ by acceleration based on Madgwick's algorithm as follows:

$$\begin{aligned} \hat{X}_{k|k-1} &= A\hat{X}_{k-1} + Bu \\ P_{k|k-1} &= AP_{k-1}A^T + Q, \end{aligned} \tag{16}$$

where

$\mathbf{u} = \begin{bmatrix} a_x \\ a_y \end{bmatrix}$, $A = \begin{bmatrix} 1 & 0 & t & 0 \\ 0 & 1 & 0 & t \\ 0 & 0 & 1 & 0 \\ 0 & 0 & 0 & 1 \end{bmatrix}$, $B = \begin{bmatrix} t^2 & 0 \\ 0 & t^2 \\ t & 0 \\ 0 & t \end{bmatrix}$ and Q is the process noise variance.

Here t is sample interval. Then we calculate the UWB location results $Y_k = \begin{bmatrix} P_{x_{UWB}} \\ P_{y_{UWB}} \end{bmatrix}$ by the RWLS algorithm as observation. The relationship between the state vector and the observed values is as follows:

$$Y_k = H\hat{X}_k, \tag{17}$$

where $H = \begin{bmatrix} 1 & 0 & 0 & 0 \\ 0 & 1 & 0 & 0 \end{bmatrix}$.

The variety of indoor environments may lead to the occurrence of non-line-of-sight ranging. Since the tag motion changes very little in a short time, we consider introducing dynamic measurement variance adjustment based on the

former position constraint. The distance between the current UWB position and the former optimal estimated position is defined as ε:

$$\varepsilon = \text{dis}\left(Y_k, \hat{X}_{k-1}(0:2)\right), \tag{18}$$

where dis() represents the distance between two points. When the ranging error is larger, the UWB positioning deviation will be larger. Then a larger measurement noise variance should be assigned. We set an empirical threshold ΔX to judge the reliability of the current measurements to dynamically adjust observation noise variance as follows:

$$R = \begin{cases} R_0, \varepsilon \leq \Delta X \\ \varepsilon \lambda R_0, \varepsilon > \Delta X \end{cases}, \tag{19}$$

where λ is the scale factor and R_0 is initial measurement noise variance. The corresponding Kalman gain is calculated according to the observation noise variance:

$$K_k = P_{k|k-1} H \left(H P_{k|k-1} H^T + R\right)^{-1}. \tag{20}$$

The state is updated with UWB location results as follows:

$$\hat{X}_k = \hat{X}_{k|k-1} + K_k \left(Y_k - \hat{X}_{k|k-1}\right). \tag{21}$$

The covariance matrix is updated as follows:

$$P_k = P_{k|k-1} - K_k P_{k|k-1}. \tag{22}$$

The complete algorithm is shown in **Adaptive Dynamic Kalman Filter algorithm**.

Adaptive Dynamic Kalman Filter algorithm

Input: $X_0, P_0, Y_k, R_0, Q, n, m, (x_i, y_i), d_{i,j}, \Delta X, \lambda$
initial position
$X_0 = \text{RWLS}\left((x_i, y_i), d_{i,j}\right), \hat{X}_0 = \left[X_0^T \ 0 \ 0\right]^T$
for $k = 1 : m$
$u =$ Madgwick's algorithm $(\text{acc}_t, gyro_t)$
Predict
$\hat{X}_{k|k-1} = A\hat{X}_{k-1} + Bu$
$P_{k|k-1} = AP_{k-1}A^T + Q$
$Y_k = \text{RWLS}\left((x_i, y_i), d_{i,j}, \hat{X}_{k-1}\right)$
Threshold judgment
If $\text{dis}\left(Y_k, \hat{X}_{k-1}(0:2)\right) > \Delta X$
    $R = \text{dis}\left(Y_k, \hat{X}_{k-1}(0:2)\right) \lambda R_0$

11: else
12: $R = R_0$
13: end
14: **Update**
15: $K_k = P_{k|k-1}H\left(HP_{k|k-1}H^T + R\right)^{-1}$
16: $\hat{X}_k = \hat{X}_{k|k-1} + K_k\left(Y_k - \hat{X}_{k|k-1}\right)$
17: $P_k = P_{k|k-1} - K_k P_{k|k-1}$
18: end
Output: $\hat{X}_k$

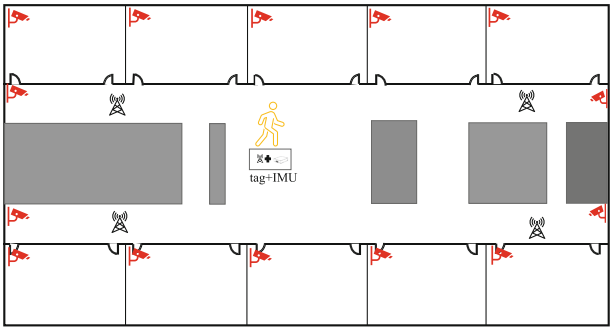

Fig. 3. The 17th floor plan of the laboratory building.

5 Implementations and Evaluations

In this section, we evaluate the performance of the proposed algorithms by experiments. Firstly, we compare the RWLS algorithm to other UWB localization algorithms (LS and WLS). Then, for the ADKF algorithm, we conduct the comparison experiment with traditional KF algorithm and the single UWB localization algorithms, and verify the practical effect of ADKF algorithm.

5.1 Experimental Setup

We evaluate our algorithms for different base station placements and multiple pedestrian movements resulting in LOS and NLOS situations. Hardware configuration has a 4-UWB anchor (MAX2000/DWM1000) and a 6-axis 1 UWB/MEMS-IMU (MPU6050) tag. Two scenarios are set up on the 17th floor of the laboratory building as shown in Fig. 3, namely scenario 1: no pedestrian movement (LOS), and scenario 2: multiple pedestrian (8–10 volunteers) movements (NLOS), which have lots of non-line-of-sight and reflection paths as shown in Fig. 1.

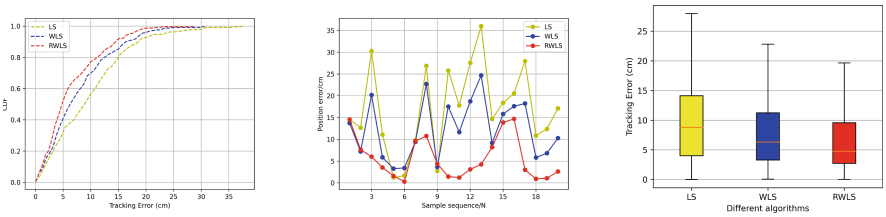

(a) CDF. (b) Location error. (c) Boxplot of error.

Fig. 4. RWLS algorithm evaluation in scenario 1.

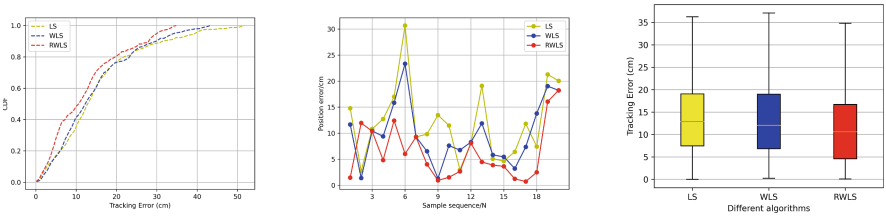

(a) CDF. (b) Location error. (c) Boxplot of error.

Fig. 5. RWLS algorithm evaluation in scenario 2.

5.2 RWLS Algorithm Evaluations

Figure 4 shows the experiment of RWLS, WLS and LS algorithms in scenario 1. In the LOS scenario, the maximum errors of RWLS, WLS and LS algorithms are 28.84 cm, 30.60 cm and 37.71 cm, respectively. The average errors of RWLS, WLS and LS algorithms are 6.25 cm, 7.83 cm and 9.67 cm respectively. The average positioning accuracy of RWLS is improved by about 35% compared with LS algorithm and improved by about 20% compared with WLS algorithm. RWLS algorithm is superior to WLS and LS as shown in the cumulative probability distribution function, error graph and boxplot. Figure 5 shows the experiment of RWLS, WLS and LS algorithms in scenario 2. In the NLOS scenario, the maximum errors of RWLS, WLS and LS algorithms are 34.82 cm, 43.71 cm and 51.70 cm, respectively. The average errors of RWLS, WLS and LS algorithms are 12.04 cm,14.30 cm and 15.04 cm respectively. The average positioning accuracy of RWLS is improved by about 20% compared with LS algorithm and improved by about 16% compared with WLS algorithm. RWLS algorithm can alleviate non-line-of-sight error very well according to the cumulative probability distribution function, error graph and boxplot.

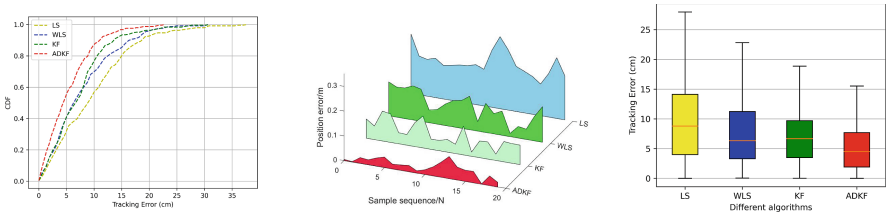

(a) CDF. (b) Location error. (c) Boxplot of error.

Fig. 6. ADKF algorithm evaluation in scenario 1.

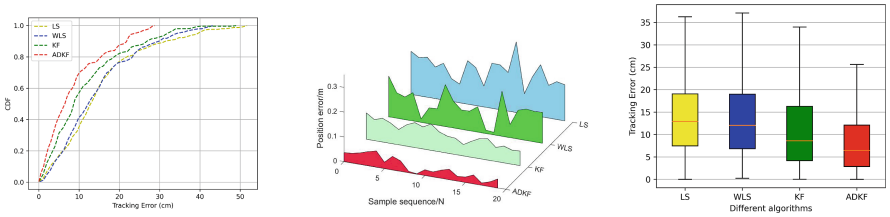

(a) CDF. (b) Location error. (c) Boxplot of error.

Fig. 7. ADKF algorithm evaluation in scenario 2.

5.3 ADKF Algorithm Evaluations

Figure 6 shows the experiment of ADKF, KF, WLS and LS algorithms in scenario 1. In the LOS scenario, the maximum errors of ADKF and KF algorithms are 22.73 cm and 30.84 cm. The average errors of ADKF and KF algorithms are 5.34 cm and 7.23 cm. Compared with the KF algorithm, the average positioning accuracy of ADKF is improved by about 26%. Further, compared with LS algorithm, ADKF algorithm effectively improves the positioning accuracy of 45%. Figure 7 shows the experiment of ADKF, KF, WLS and LS algorithms in scenario 2. In the NLOS scenario, the maximum errors of ADKF and KF algorithms are 28.76 cm and 48.98 cm. The average errors of ADKF and KF algorithms are 8.66 cm and 11.54 cm. Compared with KF algorithm, the average positioning accuracy of ADKF is improved by about 25%. Further, compared with the LS algorithm, the ADKF algorithm effectively improves the positioning accuracy of 42%. It implies that ADKF algorithm can well adapt to the dynamic changes of the environment and achieve a high positioning accuracy.

6 Conclusion

In this article, a range-constrained weighted least square (RWLS) algorithm and an adaptive dynamic Kalman Filter (ADKF) algorithm combining IMU and UWB

based on continuity of movement are proposed. Experiments show that RWLS algorithm can alleviate the non-line-of-sight positioning error due to complex indoor environments. The state equation of the KF is calculated by the data from the IMU, whereas the observation equation of the KF is calculated by the data from the UWB. The ADKF algorithm, which can effectively reduce positioning data jitter, is introduced to improve positioning accuracy. It is based on several observation BSs and an IMU. The experimental results show that our proposed RWLS algorithm clearly improves the positioning accuracy by about 20% compared to LS algorithm. Further, compared with LS algorithm, our proposed ADKF algorithm effectively improves the positioning accuracy of 42%.

Acknowledgment. This work is supported by the National Key Research and Development Program (2018YFB2100301); National Natural Science Foundation of China (61972131).

References

1. Motte, H., Wyffels, J., Strycker, L.D., Goemaere, J.P.: Evaluating GPS data in indoor environments. Adv. Electr. Comput. Eng. **11**(3), 25–28 (2011)
2. Wu, C., Xu, J., Yang, Z., Lane, N.D., Yin, Z.: Gain without pain: accurate wifi-based localization using fingerprint spatial gradient. Proc. ACM Interact. Mob. Wearable Ubiquit. Technol. **1**(2), 1–19 (2017)
3. Wu, C., Yang, Z., Xiao, C., Yang, C., Liu, Y., Liu, M.: Static power of mobile devices: self-updating radio maps for wireless indoor localization. IEEE (2015)
4. Yang, Z., Wu, C., Liu, Y.: Locating in fingerprint space: wireless indoor localization with little human intervention. In: Proceedings of the 18th Annual International Conference on Mobile Computing and Networking, pp. 269–280 (2012)
5. Yang, X., Wang, J., Song, D., Feng, B., Ye, H.: A novel NLOS error compensation method based IMU for UWB indoor positioning system. IEEE Sens. J. **21**(9), 11203–11212 (2021)
6. Cao, Y., Dhekne, A., Ammar, M.: Itracku: tracking a pen-like instrument via UWB-IMU fusion. In: Proceedings of the 19th Annual International Conference on Mobile Systems, Applications, and Services, pp. 453–466 (2021)
7. Pirsiavash, H., Ramanan, D., Fowlkes, C.C.: Globally-optimal greedy algorithms for tracking a variable number of objects. In: 2011 IEEE Conference on Computer Vision and Pattern Recognition (CVPR) (2011)
8. Rai, A., Chintalapudi, K.K., Padmanabhan, V.N., Sen, R.: Zee: zero-effort crowdsourcing for indoor localization. Microsoft Research India; Microsoft Research India; Microsoft Research India; Indian Institute of Technology, Bombay (2012)
9. Sang, C.L., Adams, M., Hesse, M., Hormann, T., Ruckert, U.: A comparative study of UWB-based true-range positioning algorithms using experimental data. In: 2019 16th Workshop on Positioning, Navigation and Communications (WPNC) (2019)
10. Li, H., Qian, Z., Tian, C., Wang, X.: TILoc: improving the robustness and accuracy for fingerprint-based indoor localization. IEEE Internet Things J. **7**(4), 3053–3066 (2020)
11. Li, Y., He, Z., Gao, Z., Zhuang, Y., Shi, C., El-Sheimy, N.: Toward robust crowdsourcing-based localization: a fingerprinting accuracy indicator enhanced wireless/magnetic/inertial integration approach. IEEE Internet Things J. **6**(2), 3585–3600 (2018)

12. Zhuang, Y., Yang, J., Qi, L., Li, Y., Cao, Y., El-Sheimy, N.: A pervasive integration platform of low-cost mems sensors and wireless signals for indoor localization. IEEE Internet Things J. **5**(6), 4616–4631 (2017)
13. Ren, C., Liu, Q., Fu, T.: A novel self-calibration method for MIMU. IEEE Sens. J. **15**(10), 5416–5422 (2015)
14. Cao, Y., Yang, C., Li, R., Knoll, A., Beltrame, G.: Accurate position racking with a single UWB anchor. In: 2020 IEEE International Conference on Robotics and Automation (ICRA), pp. 2344–2350. IEEE (2020)
15. Chandra, A., et al.: Frequency-domain in-vehicle UWB channel modeling. IEEE Trans. Veh. Technol. **65**(6), 3929–3940 (2016)
16. Wang, S., Mao, G., Zhang, J.A.: Joint time-of-arrival estimation for coherent UWB ranging in multipath environment with multi-user interference. IEEE Trans. Signal Process. **67**(14), 3743–3755 (2019)
17. Abdulrahman, A., et al.: Ultra wideband indoor positioning technologies: analysis and recent advances. Sensors **16**(5), 1–36 (2016)
18. Marano, S., Gifford, W.M., Wymeersch, H., Win, M.Z.: NLOS identification and mitigation for localization based on UWB experimental data. IEEE J. Sel. Areas Commun. **28**(7), 1026–1035 (2010)
19. Lu, Y., Yi, J., He, L., Zhu, X., Liu, P.: A hybrid fusion algorithm for integrated INS/UWB navigation and its application in vehicle platoon formation control. In: Proceedings of the 2018 International Conference on Computer Science, Electronics and Communication Engineering (CSECE 2018), Sanya, China. Atlantis Press (2018)
20. Gunia, M., Protze, F., Joram, N., Ellinger, F.: Setting up an ultra-wideband positioning system using off-the-shelf components. In: Workshop on Positioning (2016)
21. Guo, S., Zhang, Y., Gui, X., Han, L.: An improved PDR/UWB integrated system for indoor navigation applications. IEEE Sens. J. **20**(14), 8046–8061 (2020)
22. Feng, D., Wang, C., He, C., Zhuang, Y., Xia, X.G.: Kalman filter based integration of IMU and UWB for high-accuracy indoor positioning and navigation. IEEE Internet Things J. **7**(4), 3133–3146 (2020)
23. He, C., Tang, C., Yu, C.: A federated derivative cubature Kalman filter for IMU-UWB indoor positioning. Sensors **20**(12), 3514 (2020)
24. Chang, L., Li, J., Chen, S.: Initial alignment by attitude estimation for strapdown inertial navigation systems. IEEE Trans. Instrum. Meas. **64**(3), 784–794 (2014)
25. Mahony, R., Hamel, T., Pflimlin, J.M.: Nonlinear complementary filters on the special orthogonal group. IEEE Trans. Autom. Control **53**(5), 1203–1218 (2008)
26. Wang, A., Song, Y.: Improved SDS-TWR ranging technology in UWB positioning. In: 2018 International Conference on Sensor Networks and Signal Processing (SNSP) (2018)